



Cite this: *RSC Adv.*, 2024, 14, 2961

# Study of the molecular interaction of a phosphonium-based ionic liquid within myo-inositol and non-steroidal anti-inflammatory drugs

Manoj Kumar Banjare \* and Bhupendra Singh Banjare

Ionic liquids (ILs) can be used as carriers and solubilizers as well as for increasing the effectiveness of drugs. In the present investigation, the micellar properties of phosphonium-based ionic liquids (PILs) such as trihexyltetradecylphosphonium bis(2,4,4-trimethylpentyl)phosphinate ([P666(14)][THPP]) and the effect of carbocyclic sugar-based myo-inositol (MI) and non-steroidal anti-inflammatory drugs (NSAIDs), *i.e.* ibuprofen (IBU) or aspirin (ASP), on the PIL micellar system were studied using surface tension, conductivity, colorimetry, viscometry, FTIR, and dynamic light scattering (DLS) at a temperature of  $299 \pm 0.5$  K. The critical micelle concentrations (CMCs), particle size, zeta potential, and various interfacial parameters were also included *i.e.*, efficiency of adsorption ( $pC_{20}$ ), surface tension at CMC ( $\gamma_{CMC}$ ), minimum surface area per molecule ( $A_{min}$ ), surface pressure at CMC ( $\pi_{CMC}$ ), maximum surface excess concentration ( $\Gamma_{max}$ ), and various thermodynamic parameters, such as standard Gibbs free energy of adsorption ( $\Delta G_{ads}^\circ$ ), standard Gibbs free energy of micellization per alkyl tail ( $\Delta G_{tail}^\circ$ ), standard Gibbs free energy of the air–water interface ( $\Delta G_{min}^{(s)}$ ), standard Gibbs free energy of transfer ( $\Delta G_{trans}^\circ$ ), and standard Gibbs free energy of micellization ( $\Delta G_m^\circ$ ). The adsorption and micellization characteristics became more spontaneous, as shown by the more negative values of  $\Delta G_m^\circ$  and  $\Delta G_{ads}^\circ$ . Viscosity-based rheological properties were calculated for various PIL + MI and PIL + MI + NSAID systems. According to the DLS data, the PIL ( $Z = 316.4$  nm) micellar system generates substantially bigger micelles in an aqueous solution of MI + ASP ( $Z = 801.7$  nm) than in MI + IBU ( $Z = 674.7$  nm). FTIR spectroscopy revealed the interactions of PIL with MI + ASP and MI + IBU, where it was observed that MI + IBU shows good agreement with the PIL system compared to MI + ASP. The current research will have effects on pharmaceutical sciences, molecular biology, and drug delivery.

Received 11th November 2023  
Accepted 21st December 2023

DOI: 10.1039/d3ra07721g

rsc.li/rsc-advances

## 1. Introduction

Researchers are constantly working towards enhancing and improving drug delivery systems to promote the bioavailability of pharmaceuticals, reduce drug harm, and avoid adverse effects.<sup>1–4</sup> Ionic liquids (ILs) are electrolytes (co-solvents) that are also called fused salts.<sup>5,6</sup> ILs have different kinds of asymmetrical cations and symmetrical anions.<sup>7,8</sup> ILs can form of micellar nano-aggregates in aqueous solution when dissolved in water, as indicated by a decrease in surface tension.<sup>9,10</sup> ILs show unique thermal, physical, chemical and many other biological properties, which contribute significant advantages to solving some of the most critical issues facing emerging societies.<sup>11,12</sup> They are clean and efficient and are potential alternatives to volatile organic solvents (VOSs).<sup>13</sup> Phosphonium-based ionic liquids (PILs) represent the 3<sup>rd</sup> generation of ILs, and their versatility makes them indispensable,<sup>14</sup> including good

conductivity,<sup>15</sup> high thermal stability,<sup>16</sup> chemical stability,<sup>17</sup> high surface activity,<sup>18</sup> and non-flammability,<sup>19</sup> among other properties. PILs have rapidly established themselves in a wide range of applications, especially as additives in cosmetics, agrochemicals, drug delivery, and bio-extraction.<sup>20,21</sup>

Myo-inositol (MI) (cyclohexane-1,2,3,4,5,6-hexol) belongs to the cyclitols group and carbohydrates family.<sup>22,23</sup> MI is a biologically active carbocyclic sugar that acts as a signal transducer in response to hormones, neurotransmitters, and growth factors.<sup>24</sup> MI is a member of the inositol family, which has also been called cyclitols and polyols.<sup>25,26</sup> It is a primary natural product that is abundant in nature.<sup>27,28</sup> MI is used in various cosmetics, biochemical, pharmaceutical, and nutritional processes *etc.*<sup>29,30</sup>

Non-steroidal anti-inflammatory drugs (NSAIDs) help reduce inflammation, swelling, and pain. Aspirin (ASP) and ibuprofen (IBU) can be powerful lifesaving drugs that have been used for centuries to treat various ailments.<sup>31,32</sup> IBU has an amphiphilic character due to the presence of a carboxylic acid group, which has a complete hydrophobic nature.<sup>33,34</sup> When taken regularly, it can also help prevent heart attacks, strokes, and other

Department of Chemistry (MSS), MATS University, Pandri Campus, Raipur-492009, Chhattisgarh, India. E-mail: manojbanjare7@gmail.com; manojbanjarechem111@gmail.com; drmanojkb@matsuniversity.ac.in; Tel: +91-9827768119



cardiovascular conditions.<sup>35,36</sup> ASP also has antiplatelet effects, meaning it helps prevent blood clots.<sup>37</sup> It can also reduce the risk of certain cancers, such as colorectal cancer.<sup>38</sup> It can be used to treat several different conditions, including headaches, migraines, back pain, menstrual cramps, rheumatoid arthritis, and osteoarthritis.<sup>39,40</sup>

Currently, a few researchers have done studies on the interaction of myo-inositol, PIL and NSAIDs. The micellization behaviors of PIL/MI and PIL/MI/NSAIDs have many beneficial properties and are useful in many diverse fields. Panić *et al.*<sup>41</sup> studied the thermal stability and structural properties of lidocaine-based ILs, *i.e.*, lidocaine salicylate and lidocaine ibuprofenate, with ibuprofen and salicylic acid using viscosity, conductivity, IR, <sup>1</sup>H-NMR, MASS, and <sup>13</sup>C-NMR spectroscopy. By obtaining descriptors, radial distributions, and structural functions, one could understand the structural organization of synthesized ILs. Branco *et al.*<sup>42</sup> synthesized of ILs using cations such as pyridinium, ammonium and imidazolium with ibuprofen as an anion. The outcome showed that ibuprofen-based ILs have higher solubility and more effective formulations. Coutinho *et al.*<sup>43</sup> studied the aggregation behaviour of IL-drugs, such as [C<sub>4</sub>C<sub>1</sub>im][SCN] and [C<sub>4</sub>C<sub>1</sub>im][N(CN)<sub>2</sub>] with ibuprofen using dynamic light scattering (DLS) and molecular dynamics simulations (MDS). As a result, the ILs significantly increased the solubility of ibuprofen drug. Shekaari *et al.*<sup>44</sup> studied the thermodynamic properties of 1-hexyl-3-methylimidazolium bromide ([HmIm]Br) with aspirin and acetonitrile using viscosity, refractive indices, densities, and speed of sound. The cause was found in the solute-solvent interaction of aspirin and the ionic liquid.

In our previous work,<sup>45</sup> we successfully addressed the micellar behavior of conventional surfactants, *i.e.*, Triton X-100 (TX-100), cetyltrimethyl ammonium bromide (CTAB), and sodium dodecyl sulfate (SDS), in the presence of carbocyclic sugar-based myo-inositol (MI). In the present investigation, we have studied for the first time the micellar properties of a phosphonium-based ionic liquid (PIL), such as trihexyltetradecylphosphonium bis(2,4,4-trimethylpentyl)phosphinate ([P666(14)][THPP]) and investigated the molecular interaction of carbocyclic sugar-based myo-inositol (MI) with non-steroidal anti-inflammatory drugs (NSAIDs), *i.e.*, ibuprofen (IBU) and aspirin (ASP), using FTIR, surface tension, conductivity, colorimetry, viscometry, and dynamic light scattering (DLS) at a temperature of 299 ± 0.5 K. The particle size, zeta potential, critical micelle concentration (CMC), and various interfacial parameters, *i.e.*, efficiency of adsorption (pC<sub>20</sub>), surface tension at CMC (γ<sub>CMC</sub>), minimum surface area per molecule (A<sub>min</sub>), surface pressure at CMC (π<sub>CMC</sub>), maximum surface excess concentration (Γ<sub>max</sub>), and various thermodynamic parameters, such as standard Gibbs free energy of adsorption (ΔG<sub>ads</sub><sup>o</sup>), standard Gibbs free energy of micellization per alkyl tail (ΔG<sub>tail</sub><sup>o</sup>), standard Gibbs free energy of the air-water interface (ΔG<sub>min</sub><sup>o</sup>), standard Gibbs free energy of transfer (ΔG<sub>trans</sub><sup>o</sup>), and standard Gibbs free energy of micellization (ΔG<sub>m</sub><sup>o</sup>), were calculated. The PIL micellar system is utilized to develop a potential drug delivery approach for NSAIDs. Therefore, the MI + IBU system shows good agreement with the PIL system compared to

the MI + ASP system. The present paper deals with applications to drug delivery, molecular biology, and pharmaceutical sciences. Scheme 1 shows the molecular structures of PIL, myo-inositol, ibuprofen, aspirin, and methyl orange.

## 2. Experimental section

### 2.1. Materials

Trihexyltetradecylphosphonium bis(2,4,4-trimethylpentyl)phosphinate (≥99.0%), myo-inositol (≥99.0%), ibuprofen (≥98.0%), and aspirin (≥99.0%) were purchased from Sigma Aldrich Pvt. Ltd. India. Methyl orange (≥99.9%), potassium chloride (≥99.9%), and potassium bromide (≥99.9%) were purchased from Merck Mumbai, India, and ethanol (≥99.9%) from Changshu Hongsheng, China. All the chemicals were of good analytical grade. All the sample preparations were done with double-distilled water. The chemical structures are displayed in Scheme 1.

### 2.2. Methods

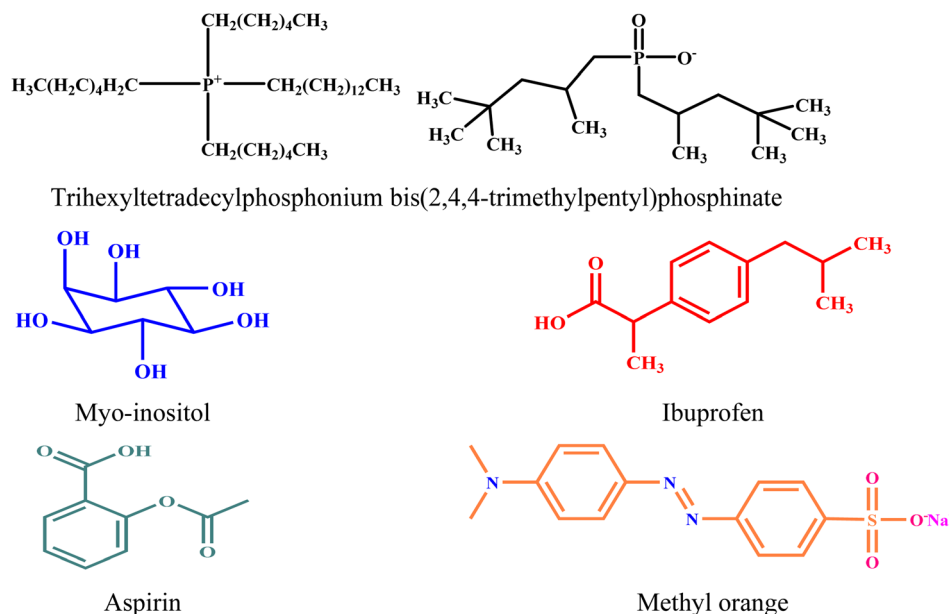
**2.2.1 Surface tension.** A stalagmometer (ABGIL Borosilicate, India) was used to determine the surface tension of [P666(14)][TMPP] and study the effect of myo-inositol (mM)/NSAIDs. The stalagmometer was calibrated using double-distilled water. The “drop counts method” was used to calculate the surface tension and CMC of [P666(14)][TMPP]/MI-NSAIDs at a temperature of 299 ± 0.5 K.

**2.2.2 Conductometry.** A study of the CMC value of the PIL, *i.e.* [P666(14)][TMPP], in the presence of myo-inositol (mM)/NSAIDs, *i.e.*, ASP or IBU, was performed using digital conductivity (ESICO International, India model Alpha-06). An aqueous solution of potassium chloride (0.1 M and 0.01 M) was used to calibrate the cell constant before each measurement. A micro-pipette was used to gradually add [P666(14)][TMPP] solution and the conductance was measured at a temperature of 299 ± 0.5 K.

**2.2.3 Colorimetry.** A digital photoelectric CL 157 (Science International Mumbai, India) colorimeter was used to investigate the confirmational CMC value of [P666(14)][TMPP] in the presence of different concentrations of myo-inositol (mM)/NSAIDs, *i.e.*, ASP and IBU. This technique is based on the Beer-Lambert law. The colorimeter absorption was calibrated using methyl orange as a probe before each measurement, and the maximum wavelength of absorption was identified at λ<sub>max</sub> = 464 nm.

**2.2.4 Viscosity.** An Ostwald viscometer (ABGIL Borosilicate, India) was used to determine the viscosity of [P666(14)][TMPP] in the presence of different concentrations of myo-inositol (mM)/NSAIDs, *i.e.*, ASP and IBU. Double-distilled water (η = 1 cp) was used to calibrate the viscometer. It was cleaned and air-dried before every use. The solution flow from the capillary for each viscosity measurement was recorded a minimum of three times using a digital stopwatch to check that the reproducibility was within ±0.01 s. The measurements were carried out at a temperature of 299 ± 0.5 K.





Scheme 1 Structures of PIL, myo-inositol, ibuprofen, aspirin, and methyl orange.

**2.2.5 Dynamic light scattering.** The size of the amphiphilic micelle was observed by dynamic light scattering (DLS) measurement performed on a Malvern Zetasizer Advanced Pro Blue UK (Model No. ZSU3200).

**2.2.6 Fourier transform infrared spectroscopy.** The Fourier transform infrared (FTIR) (Bruker, Billerica, Massachusetts, USA (Alpha-II)) spectra were taken for the systems of [P666(14)][TMPP] + MI, [P666(14)][TMPP] + MI + ASP, and [P666(14)][TMPP] + MI + IBU.

### 3. Results and discussion

#### 3.1. Study of the micellar behavior of PIL with MI and NSAIDs

Surface tension, colorimetry, conductometry, and DLS were used to investigate the micellar behavior of a PIL, *i.e.*, [P666(14)][THPP], in the presence of myo-inositol (MI)/non-steroidal anti-inflammatory drugs (NSAIDs), such as aspirin (ASP) and ibuprofen (IBU). The related results obtained using conventional and modern spectroscopic techniques reveal an extensive variety of information about the PIL with MI and NSAIDs.

In the present investigation, we studied the CMC on [P666(14)][TMPP] in the presence of different concentrations of MI/NSAIDs, *i.e.*, aspirin (ASP) or ibuprofen (IBU) using surface tension, conductivity and colorimetry measurements at  $299 \pm 0.5$  K. Table 1 and Fig. 1 show the CMC values of pure [P666(14)][TMPP], [P666(14)][TMPP] + MI + ASP and [P666(14)][TMPP] + MI + IBU systems. The CMC values are significantly reduced in the presence of MI-ASP/IBU. The MI + IBU system has a greater impact on the PIL than MI + ASP.<sup>46</sup>

**3.1.1 Surface tension.** Surface tension is a frequently employed technique for determining the characteristic properties of surface-active components. Surface tension measurements were carried out on [P666(14)][TMPP] in the presence of different

concentrations of myo-inositol (mM)/NSAIDs, such as aspirin (ASP) and ibuprofen (IBU) using stalagmometer measurement at a temperature of  $299 \pm 0.5$  K. It was found that the CMC value of native [P666(14)][TMPP] is 7.98 mM. It was observed that the CMC value of pure [P666(14)][TMPP] is reduced in the presence MI/ASP, ranging between 7.26 mM and 3.27 mM and similarly, that of the MI/IBU system ranges from 6.14 mM to 1.92 mM. The values for [P666(14)][THPP] have been significantly reduced in the presence of MI + IBU compared to MI + ASP. Because of the polar impact of MI and amphiphilic character of IBU, molecular interactions with PIL to produce CMC are conceivable even at low concentrations.<sup>47</sup> All these transformations are shown in Table 1 and Fig. 1.

**3.1.2 Conductivity.** This study began with the validation of the PIL CMC values in the presence of MI/NSAIDs at a temperature of  $299 \pm 0.5$  K. An 8.16 mM CMC value was recorded for pure PIL and this indicates that PIL has a surface active molecule. After that, the changes in CMC values of PIL in the presence of different concentrations of MI (mM)/NSAIDs, namely ASP and IBU, were determined using a conductivity technique. In Fig. 1(C) and (D), the conductance graph shows that as the free ions in a solution increase, the conductance value gradually increases. It was found that the CMC value of pure [P666(14)][TMPP] was 8.16 mM and it decreased from 7.45 mM to 2.83 mM in the MI + ASP system, and similarly in the MI + IBU system, it reduced from 5.95 mM to 1.61 mM. All transformations are shown in Fig. 1(C) and (D) and the CMC data are represented in Table 1.<sup>48</sup>

**3.1.3 Colorimetry.** Further conformational analysis of the CMC values of [P666(14)][TMPP] was undertaken using a colorimetry method. It was found that the CMC value of pure PIL is 7.98 mM, which reflects its amphiphilic character. After that, the changes in CMC values of the PIL in the presence of different concentrations of MI (mM)/5 mM of NSAIDs, *i.e.*, ASP or IBU, were determined using a colorimetry method. In this study, methyl orange was used as a probe to capture the

Table 1 CMC values of [P666(14)][THPP] in the presence of MI/NSAIDs

Myo-inositol (mM)	CMC (mM)					
	ASP (5 mM)			IBU (5 mM)		
	Surface tension	Colorimetry	Conductivity	Surface tension	Colorimetry	Conductivity
Water	7.98 ± 0.02	7.98 ± 0.02	8.16 ± 0.04	7.98 ± 0.01	7.98 ± 0.01	8.16 ± 0.02
0.5	7.26 ± 0.01	7.26 ± 0.01	7.45 ± 0.04	6.14 ± 0.02	6.20 ± 0.02	5.95 ± 0.04
1.0	5.75 ± 0.02	5.56 ± 0.01	5.36 ± 0.03	4.12 ± 0.02	4.13 ± 0.02	4.34 ± 0.03
2.0	3.27 ± 0.02	3.05 ± 0.01	2.83 ± 0.02	1.92 ± 0.02	1.92 ± 0.01	1.61 ± 0.03

absorption spectra of [P666(14)][TMPP] with MI and ASP/IBU. It was found that the CMC value of pure [P666(14)][TMPP] was 7.98 mM, and it reduced from 7.26 mM to 3.05 mM in the presence of the MI + ASP system and similarly the values for the MI + IBU system varied between 6.20 mM and 1.92 mM. All transformations are shown in Fig. 1(E) and (F) and the CMC data are represented in Table 1. Che *et al.*<sup>49</sup> performed on-site monitoring of trihexyl(tetradecyl)phosphonium fluorescein ionic liquid to trace SO<sub>2</sub> gas using fluorescent and colorimetric methods. According to the findings, colorimetric dual-signal chemosensors might be employed as smart paper labels for on-site, continuous monitoring of SO<sub>2</sub> levels in the environment.

### 3.2 Study of the interfacial parameters of PIL with MI/NSAIDs

Various interfacial properties, *i.e.*, maximum surface excess concentration ( $\Gamma_{\max}$ ), minimum surface area per molecule

( $A_{\min}$ ), surface tension at CMC ( $\gamma_{\text{CMC}}$ ), surface pressure at CMC ( $\pi_{\text{CMC}}$ ), and efficiency of adsorption ( $pC_{20}$ ) of [P666(14)][TMPP], [P666(14)][TMPP] + MI + ASP and [P666(14)][TMPP] + MI + IBU systems, were calculated using eqn (1)–(4), respectively:

$$\Gamma_{\max} = \left( \frac{1}{2.303nRT} \right) \left( \frac{d\gamma}{d \log_{10} C} \right) T_p \quad (1)$$

$$A_{\min} = \left( \frac{1}{\Gamma_{\max}} \right) N_A \quad (2)$$

$$\pi_{\text{CMC}} = \gamma_0 - \gamma_{\text{CMC}} \quad (3)$$

$$pC_{20} = -\log_{10} C_{20} \quad (4)$$

The calculated interfacial data are shown in Table 2.  $\Gamma_{\max}$  values of the higher surface activity in the MI + IBU compared to the MI + ASP system. Because of the amphiphilic nature of IBU, which together with MI leads to a tendency for PIL molecules to build up at the air–water interface, among the major group PIL

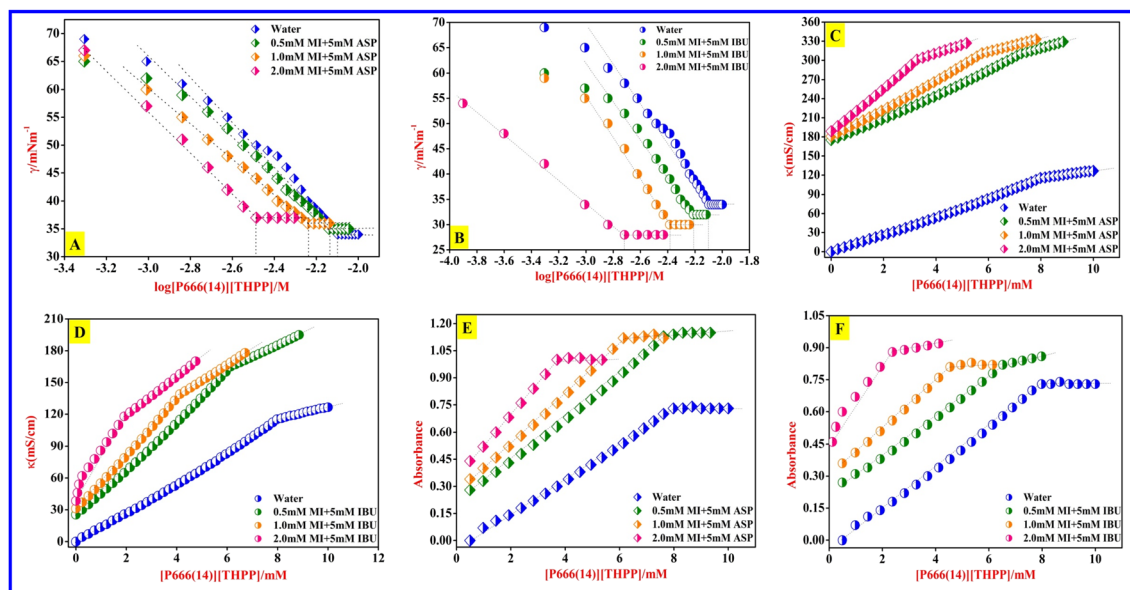


Fig. 1 [A] Plots of surface tension ( $\gamma$ ) versus the logarithm of [P666(14)][TMPP] concentration (M) in the presence of ASP. [B] Plots of surface tension ( $\gamma$ ) versus the logarithm of [P666(14)][TMPP] concentration (M) in the presence of IBU. [C] Plots of specific conductance ( $\kappa$ ) versus concentration of [P666(14)][TMPP] (mM) in the presence of ASP. [D] Plots of specific conductance ( $\kappa$ ) versus concentration of [P666(14)][TMPP] (mM) in the presence of IBU. [E] Plots of absorbance versus concentration of [P666(14)][TMPP] (mM) in the presence of ASP. [F] Plots of absorbance versus concentration of [P666(14)][TMPP] (mM) in the presence of IBU.





and MI will be more effective due to the counter-ion–polar interaction.<sup>50</sup> The  $A_{\min}$  values of [P666(14)][TMPP] + MI + ASP and [P666(14)][TMPP] + MI + IBU rose when a mixed solution formed a loose mixed monolayer at the surface. However, the influence of MI + IBU was revealed, due to which the available surface area for PIL molecules was diminished. The highest values of  $\pi_{\text{CMC}}$  in MI-IBU indicate more effective adsorption at the interface of PIL due to the cation–anion repulsion of IL being larger than the cation–anion repulsion of ASP.

Thus, the larger hydrophilic head part of the system will exhibit greater repulsion at the interface. The  $pC_{20}$  value shows the adsorption effectiveness at the air/water interface of the [P666(14)][TMPP] + MI + ASP and [P666(14)][TMPP] + MI + IBU systems. The  $pC_{20}$  value is following decreasing order: MI + IBU > MI + ASP. As previously reported, our research group (Banjare *et al.*<sup>51</sup>) examined the physicochemical properties of sodium dodecyl sulfate (SDS) and Triton X-100 with trihexyltetradecylphosphonium bis(2,4,4-trimethylpentyl)phosphinate ionic liquid and further used these systems to explore combinations with paracetamol (PCM) for potential benefit with the help of surface tension, FTIR, colorimetry, and viscometry techniques. The outcome of the study is that the Triton X-100 system exhibits higher binding affinity for PCM drugs than the SDS system.

### 3.3 Study of the critical packing parameter of PIL with MI/NSAIDs

The critical packing parameter ( $P$ ) of PIL [P666(14)][TMPP], [P666(14)][TMPP] + MI + ASP and [P666(14)][TMPP] + MI + IBU systems was calculated by using eqn (5)–(7).

$$P = \frac{V_0}{A_{\min}l_c} \quad (5)$$

$$V_0 = (27.4 + 26.9C_n) \text{ \AA}^3 \text{ per hydrocarbon chain} \quad (6)$$

$$l_c = (1.5 + 1.265C_n) \text{ \AA} \text{ per hydrocarbon chain} \quad (7)$$

The value of  $P$  is  $\leq 0.33$  for a spherical micelle. The mixed systems of MI + ASP and MI + IBU with PIL show that the shape of the aggregate system changes from globular to spherical with increasing concentration.<sup>52</sup> All the transformations are reported in Table 2 and Fig. 2.

### 3.4 Study of the thermodynamic parameters of PIL with MI/NSAID

The molecular adsorption and micellization behavior, *i.e.*, degree of micellar ionization ( $\alpha$ ), counter-ion binding ( $\beta$ ), standard Gibbs free energy of transfer ( $\Delta G_{\text{trans}}^\circ$ ), standard Gibbs free energy of adsorption ( $\Delta G_{\text{ads}}^\circ$ ), standard Gibbs free energy of micellization ( $\Delta G_{\text{m}}^\circ$ ), standard Gibbs free energy of the air–water interface ( $\Delta G_{\text{min}}^{(s)}$ ), and standard Gibbs free energy of micellization per alkyl tail ( $\Delta G_{\text{tail}}^\circ$ ), were calculated for [P666(14)][THPP] in the presence of different concentrations of MI/ASP/IBU at a temperature of  $299 \pm 0.5$  K and the data are shown in Table 3. All the thermodynamic parameters were computed with the help of eqn (8)–(13).

$$\alpha = \frac{S_2}{S_1} \quad (8)$$

$$\Delta G_{\text{M}}^\circ = (2 - \alpha)RT \ln \frac{55.4}{\text{CMC}} \quad (9)$$

$$\Delta G_{\text{ads}}^\circ = \Delta G_{\text{M}}^\circ - \frac{\pi_{\text{CMC}}}{\Gamma_{\text{max}}} \quad (10)$$

$$\Delta G_{\text{trans}}^\circ = \Delta G_{\text{M}(\text{solvents mixed media})}^\circ - \Delta G_{\text{M}(\text{pure water})}^\circ \quad (11)$$

$$\Delta G_{\text{min}}^{(s)} = A_{\min} \times \gamma_{\text{CMC}} \times N_A \quad (12)$$

$$\Delta G_{\text{m,tail}}^\circ = \frac{\Delta G_{\text{M}}^\circ}{2} \quad (13)$$

The  $\alpha$  value shown by the PIL + MI + IBU system undergoes a comparatively higher change than the PIL + MI + ASP system. An accumulation of counter-ions on the polar shell of the micelle, along with the electrostatic attraction between negative and positive charges, happens due to hydrogen bonding between MI and its phosphonium ion, as shown in Scheme 2. The  $\Delta G_{\text{m}}^\circ$  of the [P666(14)][TMPP] + MI + ASP and [P666(14)][TMPP] + MI + IBU systems show negative values and are quite similar for both systems. This shows that the micellization process is spontaneous.<sup>53</sup> The  $\Delta G_{\text{ads}}^\circ$  of MI–ASP/IBU also indicate a spontaneous micellization process in the system of PIL. The maximum  $\Delta G_{\text{ads}}^\circ$  negative value was recorded in the PIL +

**Table 2** Various interfacial parameters, *i.e.*, surface tension ( $\gamma$ ), surface pressure at CMC ( $\pi_{\text{CMC}}$ ), efficiency of adsorption ( $pC_{20}$ ), minimum surface area per molecule ( $A_{\min}$ ), and maximum surface excess concentration ( $\Gamma_{\text{max}}$ ) of [P666(14)][THPP] with MI/NSAIDs

Myo-inositol (mM)	$\gamma_{\text{CMC}}$ (mN m <sup>−1</sup> )	$\Gamma_{\text{max}}$ (mol m <sup>−2</sup> ) 10 <sup>6</sup>	$A_{\min}$ (m <sup>2</sup> mol <sup>−1</sup> )	$\pi_{\text{CMC}}$ (mN m <sup>−1</sup> )	$pC_{20}$	CPP ( $P$ )
<b>ASP (5 mM)</b>						
Water	34 ± 0.05	3.08 ± 0.07	53.89 ± 0.08	38 ± 0.05	2.60 ± 0.05	0.40 ± 0.03
0.5	35 ± 0.04	2.49 ± 0.05	66.67 ± 0.09	37 ± 0.03	2.73 ± 0.06	0.32 ± 0.08
1.0	36 ± 0.06	2.46 ± 0.03	67.24 ± 0.04	36 ± 0.06	2.80 ± 0.07	0.32 ± 0.04
2.0	37 ± 0.03	2.79 ± 0.06	59.39 ± 0.06	35 ± 0.05	2.95 ± 0.08	0.36 ± 0.06
<b>IBU (5 mM)</b>						
Water	34 ± 0.05	3.08 ± 0.04	53.89 ± 0.04	38 ± 0.09	2.60 ± 0.02	0.40 ± 0.07
0.5	32 ± 0.06	2.51 ± 0.05	66.10 ± 0.05	40 ± 0.06	2.90 ± 0.05	0.32 ± 0.08
1.0	30 ± 0.08	2.80 ± 0.09	59.21 ± 0.08	42 ± 0.04	3.07 ± 0.08	0.36 ± 0.04
2.0	28 ± 0.07	1.65 ± 0.08	100.51 ± 0.07	44 ± 0.05	3.98 ± 0.06	0.21 ± 0.03



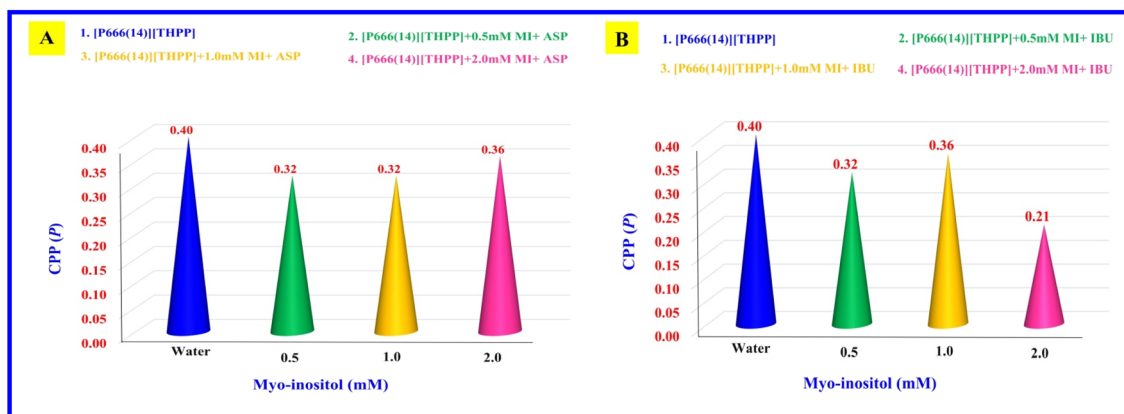


Fig. 2 Graphs plotted between the critical packing parameter ( $P$ ) and concentration of myo-inositol (mM): (A) [P666(14)][THPP] + MI + ASP, (B) [P666(14)][THPP] + MI + IBU.

MI + IBU system compared to PIL + MI + ASP, as shown in Table 3. When employing PIL-ASP/IBU with various MI concentrations (mM), the  $\Delta G_{\text{trans}}^{\circ}$  have proven to be more advantageous for forming bulk-phase assemblies. It has been established that  $\Delta G_{\text{trans}}^{\circ}$  indicate micellization of PIL in mixed environments and that in their important interactions with ASP and IBU in increased concentrations of MI (mM), the  $\Delta G_{\text{trans}}^{\circ}$  have shown a more negative trend in the PIL + MI + ASP system compared to PIL + MI + IBU.

A greater change in the  $\Delta G_{\text{min}}^{(s)}$  value at the air–water interface was seen as the bulk phase changed to the surface phase of the PIL + MI + IBU system. Due to the lowest free energy, the air–water interfaces have excellent thermodynamic stability. In PIL, the  $\Delta G_{\text{m,tail}}^{\circ}$  is out of contact with solvent mixtures. Based on the standard Gibbs free energy exchange between pure water and PIL, it has been established that MI–ASP/IBU produces a solvophobic effect.<sup>54</sup>

### 3.5 Study the viscosity of PIL-MI with NSAID systems

Viscometry is a reliable technique for testing the quality of drugs and it is used significantly to test the conformational and rheological changes in solvents that exhibit viscosity characteristics. The initially different viscosity parameters, such as relative, reduced, and intrinsic viscosity, were determined for [P666(14)]

[TMPP] at different concentrations of MI (mM) solution. Similarly, the rheological parameters of [P666(14)][TMPP] in the presence of MI–ASP/IBU systems were investigated using the viscosity method. The relative viscosity of [P666(14)][TMPP] with MI–ASP/IBU systems was identified from eqn (14). The  $\eta_{\text{red}}$  was calculated from eqn (15) and (16).

$$\eta_r = \frac{\eta_s}{\eta_0} \quad (14)$$

$$\eta_{\text{red}} = \frac{\eta_{\text{sp}}}{C} \quad (15)$$

$$\eta_{\text{sp}} = \eta_r - 1 \quad (16)$$

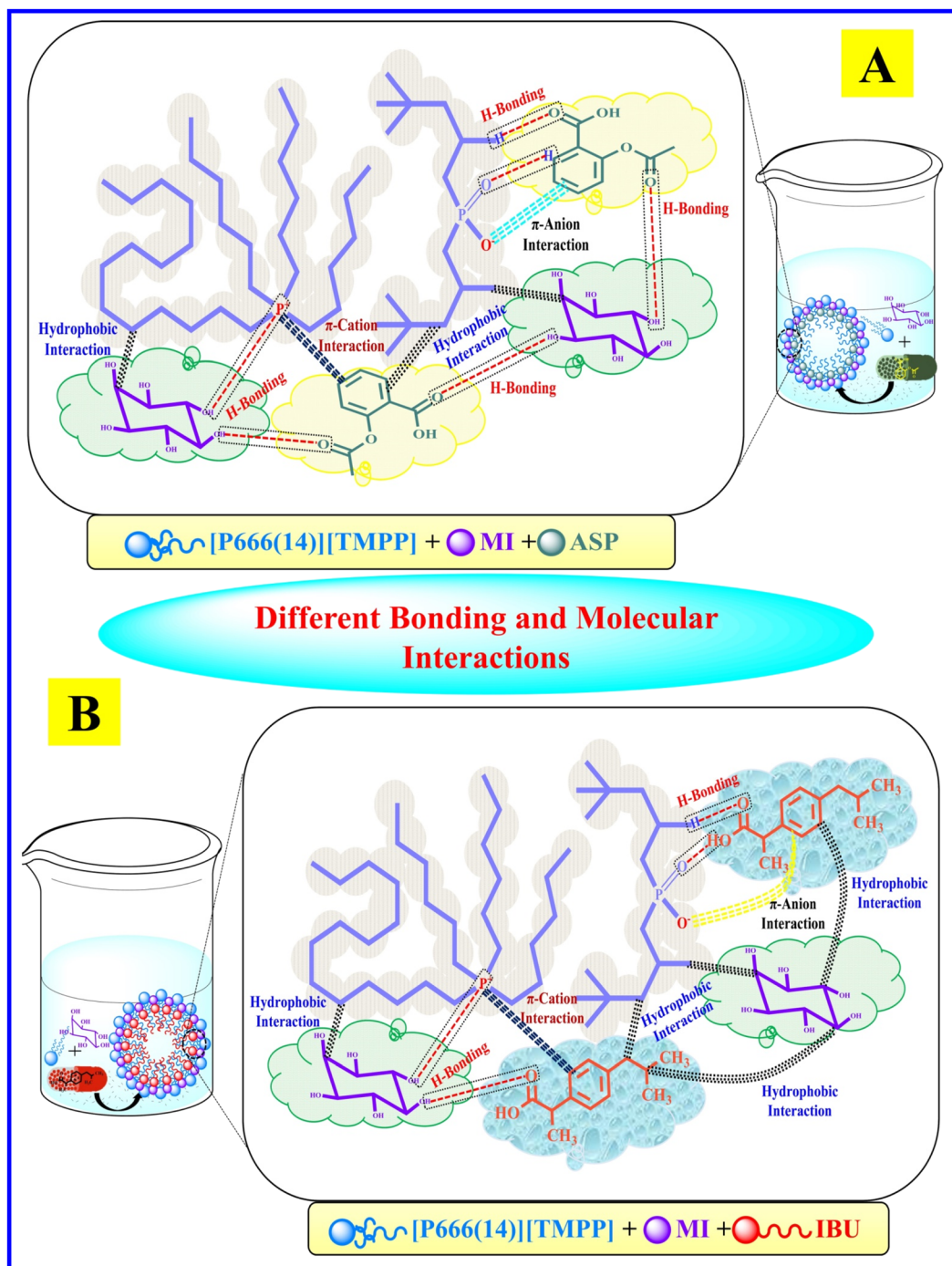
$$[\eta] = \lim_{C \rightarrow 0} \frac{\eta_{\text{sp}}}{C} \quad (17)$$

The  $[\eta]$  of each system was calculated from eqn (17). For the activity on the [P666(14)][TMPP] + MI + ASP and [P666(14)][TMPP] + MI + IBU systems, the raised  $[\eta]$  value indicates that the micelle of bulky phosphonium ions has stretched at high MI concentrations. According to Fig. 3(F), increasing  $[\eta]$  values near the inflection point at 0.5 mM suggest that PIL expansion has formed micelles. Stronger electrostatic attraction is the most likely cause of this expansion of conformation.<sup>55</sup> At this stage, the MI–ASP/IBU

Table 3 Various calculated thermodynamic parameters of [P666(14)][TMPP]–MI/NSAIDs, such as aspirin (ASP) or ibuprofen (IBU) at a temperature of  $299 \pm 0.5$  K

Myo-inositol (mM)	$\alpha$	$\beta$	$\Delta G_{\text{m}}^{\circ}$ (kJ mol <sup>−1</sup> )	$\Delta G_{\text{ads}}^{\circ}$ (kJ mol <sup>−1</sup> )	$\Delta G_{\text{trans}}^{\circ}$ (kJ mol <sup>−1</sup> )	$\Delta G_{\text{min}}^{(s)}$ (kJ mol <sup>−1</sup> )	$\Delta G_{\text{m,tail}}^{\circ}$ (kJ mol <sup>−1</sup> )
<b>ASP (5 mM)</b>							
Water	$0.14 \pm 0.02$	$0.86 \pm 0.02$	$-22.29 \pm 0.02$	$-34.63 \pm 0.02$	—	$11.03 \pm 0.01$	$-11.14 \pm 0.02$
0.5	$0.18 \pm 0.03$	$0.82 \pm 0.03$	$-22.34 \pm 0.02$	$-37.20 \pm 0.02$	$-0.08 \pm 0.02$	$14.05 \pm 0.04$	$-11.17 \pm 0.03$
1.0	$0.17 \pm 0.05$	$0.83 \pm 0.05$	$-23.54 \pm 0.02$	$-38.17 \pm 0.01$	$-1.27 \pm 0.02$	$14.57 \pm 0.02$	$-11.77 \pm 0.03$
2.0	$0.15 \pm 0.03$	$0.85 \pm 0.01$	$-26.58 \pm 0.01$	$-39.13 \pm 0.01$	$-4.32 \pm 0.02$	$13.23 \pm 0.02$	$-13.29 \pm 0.02$
<b>IBU (5 mM)</b>							
Water	$0.14 \pm 0.01$	$0.86 \pm 0.02$	$-22.29 \pm 0.02$	$-34.63 \pm 0.03$	—	$11.03 \pm 0.01$	$-11.14 \pm 0.01$
0.5	$0.19 \pm 0.03$	$0.81 \pm 0.04$	$-22.98 \pm 0.03$	$-38.91 \pm 0.01$	$-0.68 \pm 0.02$	$12.73 \pm 0.02$	$-11.49 \pm 0.02$
1.0	$0.23 \pm 0.05$	$0.77 \pm 0.05$	$-24.21 \pm 0.02$	$-39.21 \pm 0.02$	$-1.91 \pm 0.03$	$10.69 \pm 0.01$	$-12.10 \pm 0.03$
2.0	$0.34 \pm 0.02$	$0.66 \pm 0.03$	$-25.89 \pm 0.02$	$-52.56 \pm 0.01$	$-3.59 \pm 0.02$	$16.94 \pm 0.01$	$-12.94 \pm 0.01$





Scheme 2 A systematic representation of different bonding and molecular interactions of [A] [P666(14)][TMPP] + MI + ASP and [B] [P666(14)][TMPP] + MI + IBU.

system may be thought of as consisting of micelles that have been linked to [P666(14)][THPP]. Each parameter has been transformed and is shown in Fig. 3.

### 3.6 Study of dynamic light scattering of PIL with MI/NSAIDs systems

Dynamic light scattering (DLS) is a prominent technique for particle size analysis of the micellar system of PIL [P666(14)]

[THPP] and that mixed with 2 mM concentration of MI, respectively, and the data are reported in Table 4 and Fig. 4. DLS analyzed the micellar aggregates of [P666(14)][THPP] + MI + ASP, [P666(14)][THPP] + MI + IBU and the size was determined by the hydrodynamic diameter. The average radius of the [P666(14)][THPP] + MI + ASP system shows a polymodal distribution and its hydrodynamic radii ( $R_h$ ) are 169.9, 893.8, 5468 (d.nm) and PDI = 0.7693. The average radius of the [P666(14)]



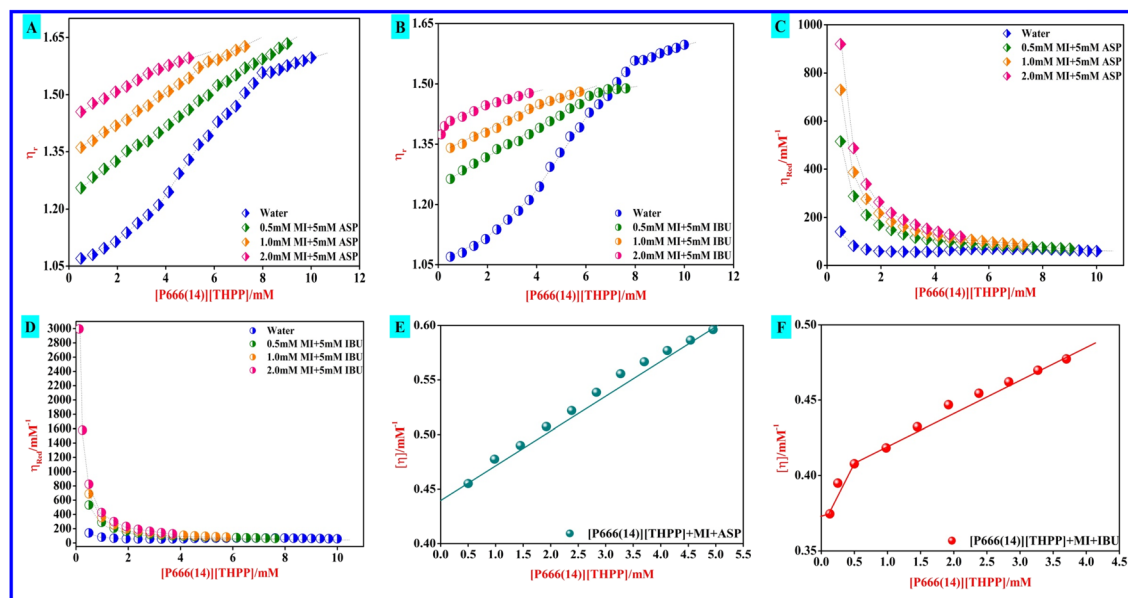


Fig. 3 [A] Plots of relative viscosity ( $\eta_r$ ) versus concentration of [P666(14)][THPP] (mM) with ASP NSAIDs in the presence of myo-inositol (MI) (mM). [B] Plots of relative viscosity ( $\eta_r$ ) versus concentration of [P666(14)][THPP] (mM) with IBU NSAIDs in the presence of myo-inositol (MI) (mM). [C] Plots of reduced viscosity ( $\eta_{red}$ ) versus concentration of [P666(14)][THPP] (mM) with ASP NSAIDs in the presence of myo-inositol (MI) (mM). [D] Plots of reduced viscosity ( $\eta_{red}$ ) versus concentration of [P666(14)][THPP] (mM) with IBU NSAIDs in the presence of myo-inositol (MI) (mM). [E] Intrinsic viscosity  $[\eta]$  vs. concentration of [P666(14)][THPP] (mM) with ASP in the presence of 2 mM concentration of MI, [F] intrinsic viscosity  $[\eta]$  vs. concentration of [P666(14)][THPP] (mM) with IBU in the presence of 2 mM concentration of MI.

[THPP] + MI + IBU system shows a bimodal distribution and the hydrodynamic radii ( $R_h$ ) are 79.88, 420.2 (d.nm) and PDI = 0.5053. In general, the findings of the studies indicate that micelle-like aggregates can develop even when MI is present.<sup>56</sup>

### 3.7 Zeta potential study of PIL-MI with NSAID systems

The difference in the micellization potential value of [P666(14)][THPP] in aqueous solution and MI-ASP/IBU systems was determined using the DLS technique and the zeta potential ( $\zeta$ ) value of [P666(14)][THPP] is observed at  $-16.79$  mV. We measured the zeta potential diffuse and Stern layers of a particle's surface charge and their relationship with dispersed aggregation. Fig. 5 and Table 4 show the zeta ( $\zeta$ ) potential data of pure [P666(14)][THPP], [P666(14)][THPP] + MI + ASP and [P666(14)][THPP] + MI + IBU systems.

The value of  $\zeta$  potential (mV) significantly changes to a negative value with the addition of MI on [P666(14)][THPP] when the  $\zeta$  value changes from  $-16.79$  mV to  $-28.70$  mV; with the MI + ASP system, the  $\zeta$  value is changed from  $-16.79$  mV to  $-27.87$  mV and the MI + IBU system, the  $\zeta$  value is changed

from  $-16.79$  mV to  $-19.59$  mV. The micellar system PIL + MI + ASP exhibits substantial electrostatic stabilization due to its high negative charge. A system-charged species distribution may have contributed to the observed significant electrostatic stabilization. Consequently, the outcome of every system has exhibited diverse particle morphologies that self-assemble as a result of a decrease in negative  $\zeta$  potential values.<sup>57</sup>

### 3.8 FTIR study of PIL with MI and NSAID

The FTIR technique may provide significant information about the molecular interaction of native PIL, *i.e.* [P666(14)][THPP] and mixed systems of myo-inositol, and ASP/IBU. IR band shifts are reported in both systems due to different types of possible molecular interaction between the PIL with MI and NSAIDs, indicating the formation of various bonds through out the system, such as  $\pi$ -bond-cation interaction, hydrogen bonding, electrostatic interactions, hydrophobic interactions, and van der Waals interactions, as shown in Scheme 2. The stretching frequency of native and mixed IR spectra is summarized in Table 5. Banjare *et al.*<sup>58</sup> explored the formation of an inclusion complex (IC) between trihexyltetradecylphosphonium bis(2,4,4-trimethylpentyl)phosphinate and  $\beta$ -cyclodextrin and further binding of paracetamol drug with the help of FTIR and UV-visible spectroscopy. The outcome is that the IC has significantly improved the binding capacity of the paracetamol drug.

**3.8.1 IR spectra of native [P666(14)][THPP].** The IR spectra of pure PIL [P666(14)][THPP] data are shown in Table 5. The small [O-H] stretching bands of PIL are observed at  $3682\text{ cm}^{-1}$

Table 4 Z-Average,  $R_h$  (nm), PDI and zeta potential ( $\zeta$ ) values of pure and 2 mM concentrations of MI/(ASP/IBU) with [P666(14)][THPP]

Micellar systems PIL	PDI	$R_h$ (nm)	Z-Average	$\zeta$ (mV)
Water	0.6279	267.2, 5468	316.4	$-16.79$
2 mM MI	0.9286	125.6, 768.5, 5468	563.2	$-28.70$
2 mM MI + 5 mM ASP	0.7693	169.9, 893.8, 5468	801.7	$-27.87$
2 mM MI + 5 mM IBU	0.5053	79.88, 420.2	674.7	$-19.59$





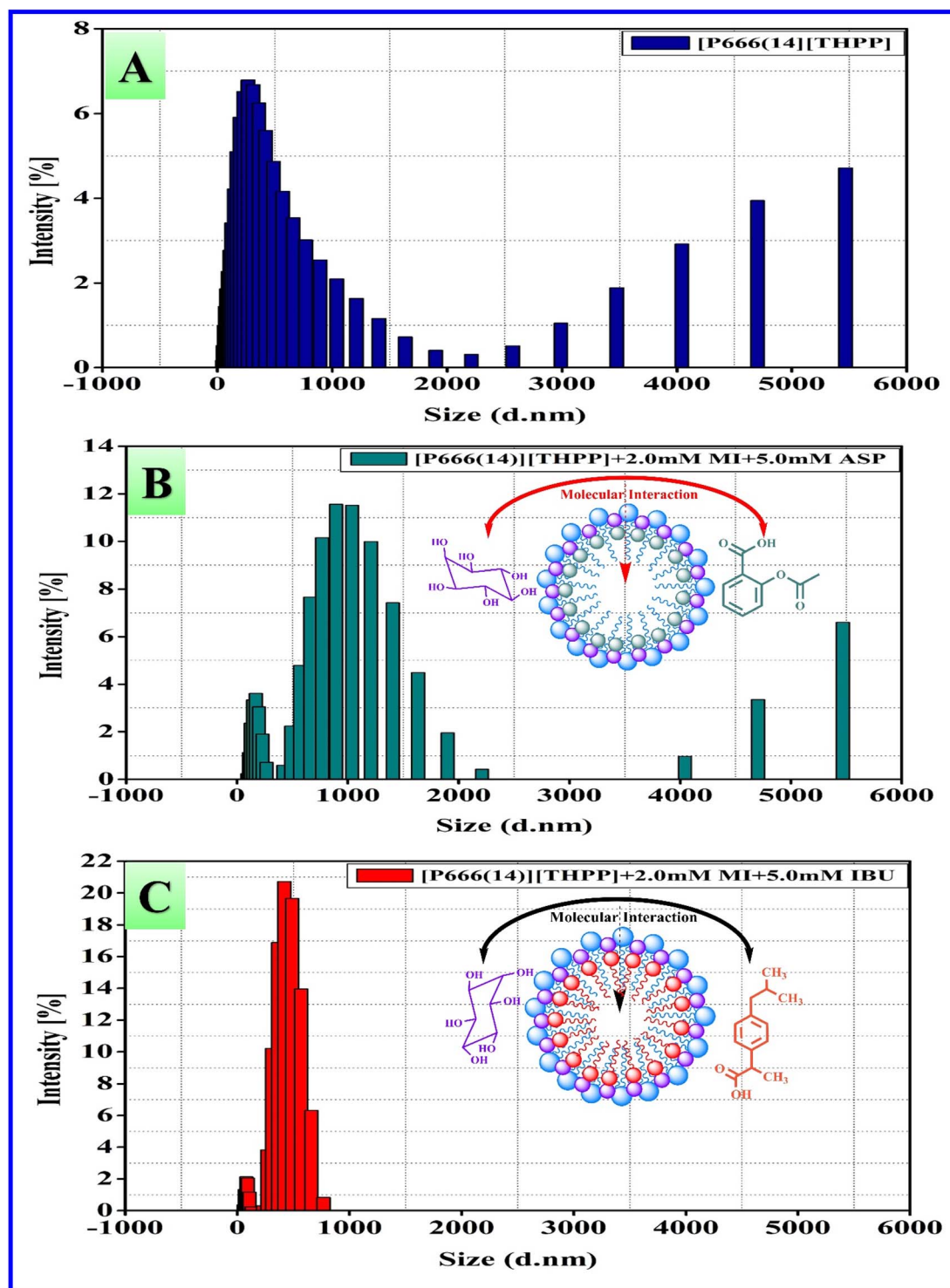


Fig. 4 Particle size distribution determined by DLS for [P666(14)][THPP] with 5 mM ASP and IBU in the presence of 2 mM myo-inositol (MI): [A] [P666(14)][THPP], [B] [P666(14)][THPP] + MI + ASP, and [C] [P666(14)][THPP] + MI + IBU.

and  $3175\text{ cm}^{-1}$ . The sharp peak of [O-H] bending is observed at  $1364\text{ cm}^{-1}$ . The long-chain symmetric and asymmetric [C-H] stretching bands are observed at  $2925\text{ cm}^{-1}$  and  $2854\text{ cm}^{-1}$ . The phosphonium ion [P=O] stretching bands are observed at  $1166\text{ cm}^{-1}$  and  $1024\text{ cm}^{-1}$ . The phosphonium ion [P-O-P]

stretching band is observed at  $1654\text{ cm}^{-1}$ . The long carbon chain [C-H] in-plane bending of PIL is observed at  $1463\text{ cm}^{-1}$  and [C=C] bending is observed at  $806\text{ cm}^{-1}$ .

**3.8.2 IR spectra of native aspirin and ibuprofen.** The NSAIDs of pure aspirin and ibuprofen spectra are shown in

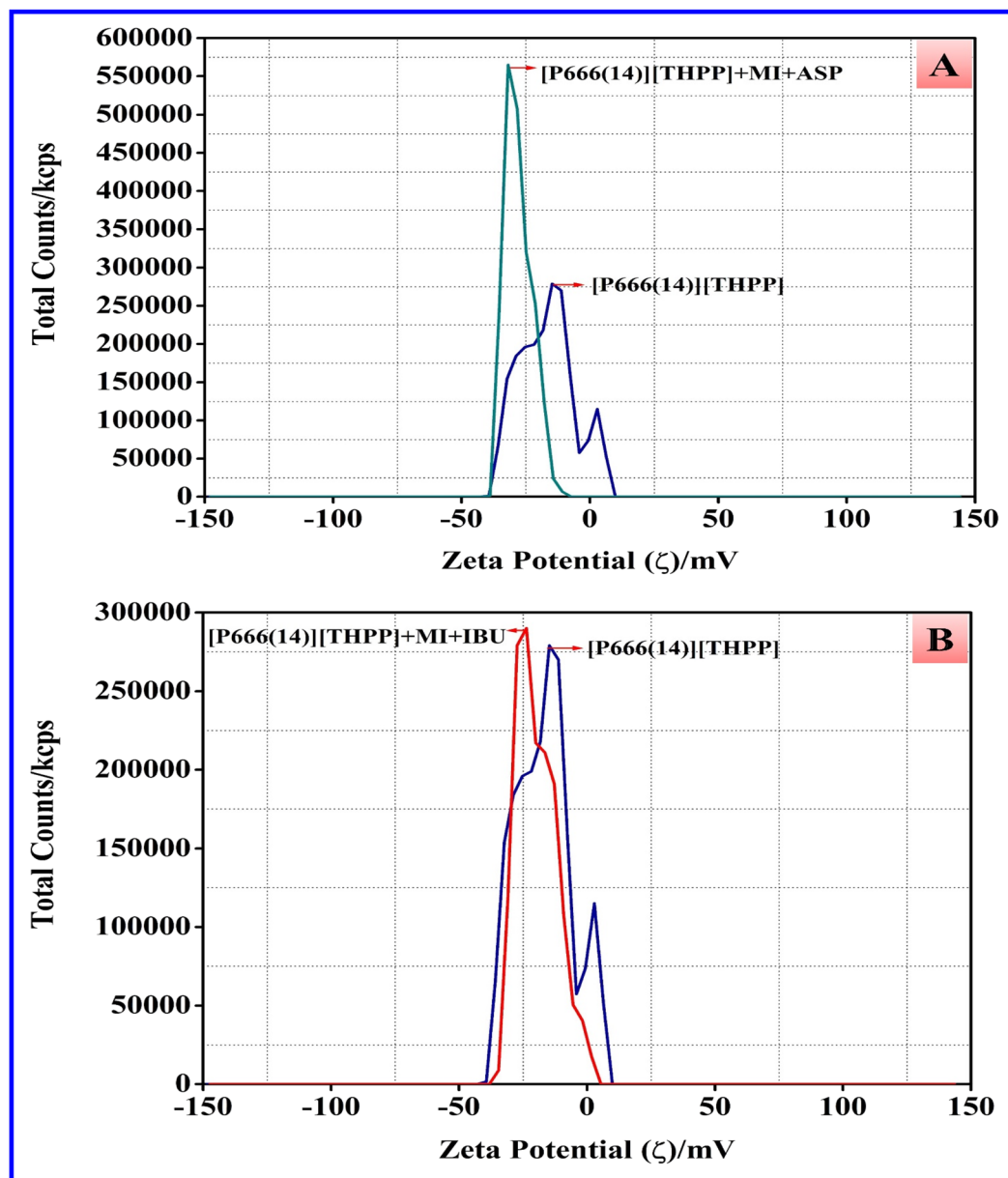


Fig. 5 [A] Zeta potential ( $\zeta$ ) data of [P666(14)][THPP] with 5 mM ASP in the presence of 2 mM myo-inositol (MI). [B] Zeta potential ( $\zeta$ ) data of [P666(14)][THPP] with 5 mM IBU in the presence of 2 mM myo-inositol (MI).

Table 5 and Fig. 6(B) and (D). The carboxylic group containing [O–H] stretching (broad) bands are observed at  $2831\text{ cm}^{-1}$  and  $2699\text{ cm}^{-1}$  for ASP and  $3783\text{ cm}^{-1}$ ,  $3679\text{ cm}^{-1}$ , and  $3092\text{ cm}^{-1}$  for IBU. The symmetric and asymmetric [C–H] stretching bands are observed at  $2547\text{ cm}^{-1}$  for ASP and at  $2952\text{ cm}^{-1}$ ,  $2921\text{ cm}^{-1}$  and  $2870\text{ cm}^{-1}$  for IBU. The sharp peak [O–H] bending is observed at  $1305\text{ cm}^{-1}$  for ASP and at  $1231\text{ cm}^{-1}$  for IBU. The carboxylic and ester group with [C=O] stretching bands are observed at  $1745\text{ cm}^{-1}$  and  $1676\text{ cm}^{-1}$  for ASP and  $1708\text{ cm}^{-1}$  for IBU. The aromatic methylene ring containing [C–H] bending is observed at  $1455\text{ cm}^{-1}$  for ASP and at  $1422\text{ cm}^{-1}$  for IBU. The [C–O] stretching band is observed at  $1182\text{ cm}^{-1}$  for ASP and at  $1006\text{ cm}^{-1}$  for IBU. The aromatic ring [C=C] bending spectra are observed at  $835\text{ cm}^{-1}$  and the [C–H] bending (disubstituted

benzene) is observed at  $754\text{ cm}^{-1}$  for ASP and at  $860\text{ cm}^{-1}$  and  $777\text{ cm}^{-1}$  for IBU.

**3.8.3 IR spectra of the mixed [P666(14)][TMPP] + MI + ASP system.** FTIR spectra of [P666(14)][TMPP], MI and ASP systems are shown in Fig. 6(A) and Table 5. The [O–H] stretching band is observed at  $3682\text{ cm}^{-1}$  and is shifted to  $3666\text{ cm}^{-1}$ , which indicates a  $26\text{ cm}^{-1}$  shift in IR frequency. The [O–H] bending is observed at  $1364\text{ cm}^{-1}$  and is shifted to  $1301\text{ cm}^{-1}$ , which indicates a  $63\text{ cm}^{-1}$  shift in IR frequency. The long-chain symmetric and asymmetric [C–H] stretching bands are observed at  $2925$  and  $2854\text{ cm}^{-1}$  and are shifted to  $2926\text{ cm}^{-1}$  and  $2858\text{ cm}^{-1}$ , which indicates  $1\text{ cm}^{-1}$  and  $4\text{ cm}^{-1}$  shifts in IR frequency, respectively. The carboxylic and ester groups with [C=O] stretching bands are observed at  $1745\text{ cm}^{-1}$  and



Table 5 IR absorption bands of [P666(14)][TMPP], ASP, IBU, [P666(14)][THPP] + MI + ASP and [P666(14)][THPP] + MI + IBU

Functional group	Wavenumber (cm <sup>-1</sup> )				
	[P666(14)][TMPP] pure	ASP pure	[P666(14)][TMPP] + MI + ASP	IBU pure	[P666(14)][TMPP] + MI + IBU
[O-H] stretching bands	3682	—	3666	3783	3778
	3175	—	—	3679	3456
[O-H] bending	1364	1305	1301	1231	1220
[C-H] stretching bands	2925	2547	2926	2952	2923
	2854	—	2858	2921	2859
[C=O] stretching bands	—	1745	1664	2870	1710
	—	1676	1600	1708	—
[C-O], [C-O-C], [P=O] stretching bands	1166	1182	1111	1006	1091
	1024	—	1027	—	1049
[C-H] bending	1463	1455	1469	1422	1470
[C=C] bending	806	835	848	860	857
[C-H] bending (disubstituted benzene)	—	754	757	777	809

1676 cm<sup>-1</sup> and are shifted to 1664 cm<sup>-1</sup> and 1600 cm<sup>-1</sup>, which indicates 81 cm<sup>-1</sup> and 76 cm<sup>-1</sup> shifts in IR frequency, respectively. The [C-O] stretching band is observed at 1182 cm<sup>-1</sup> and is shifted to 1111 cm<sup>-1</sup> and 1027 cm<sup>-1</sup>, which indicates a 71 cm<sup>-1</sup> shift in IR frequency. The long carbon chain [C-H] bending is observed at 1463 cm<sup>-1</sup> and is shifted to 1469 cm<sup>-1</sup>, which indicates a 6 cm<sup>-1</sup> shift in IR frequency. The [C=C] bending is observed at 806 cm<sup>-1</sup> and is shifted to 848 cm<sup>-1</sup>, which indicates a 42 cm<sup>-1</sup> shift in IR frequency. The [C-H] bending (disubstituted benzene) is observed at 754 cm<sup>-1</sup> and is shifted to 757 cm<sup>-1</sup>, which indicates a 3 cm<sup>-1</sup> shift in IR frequency.

**3.8.4 IR spectra of the mixed [P666(14)][TMPP] + MI + IBU system.** FTIR spectra of [P666(14)][TMPP], MI and IBU are shown in Fig. 6(C) and Table 5. The [O-H] stretching bands are

observed at 3783 cm<sup>-1</sup>, and 3679 cm<sup>-1</sup> and are shifted to 3778 cm<sup>-1</sup> and 3456 cm<sup>-1</sup>, which indicates 5 cm<sup>-1</sup> and big 223 cm<sup>-1</sup> shifts in IR frequency. The [O-H] bending is observed at 1364 cm<sup>-1</sup> and is shifted to 1220 cm<sup>-1</sup>, which indicates a big 144 cm<sup>-1</sup> shift in IR frequency. The long-chain symmetric and asymmetric [C-H] stretching bands are observed at 2952 cm<sup>-1</sup>, 2921 cm<sup>-1</sup>, and 2870 cm<sup>-1</sup> and are shifted to 2923 cm<sup>-1</sup> and 2859 cm<sup>-1</sup>, which indicates 29 cm<sup>-1</sup> and 11 cm<sup>-1</sup> shifts in IR frequency. The carboxylic group [C=O] stretching band is observed at 1708 cm<sup>-1</sup> and is shifted to 1710 cm<sup>-1</sup>, which indicates a 2 cm<sup>-1</sup> shift in IR frequency. The [C-O] stretching bands are observed at 1166 cm<sup>-1</sup> and 1024 cm<sup>-1</sup> and are shifted to 1091 cm<sup>-1</sup> and 1049 cm<sup>-1</sup>, which indicates 75 cm<sup>-1</sup> and 25 cm<sup>-1</sup> shifts in IR frequency. The long carbon chain [C-H] bending is observed at 1463 cm<sup>-1</sup> and is shifted to 1470 cm<sup>-1</sup>,

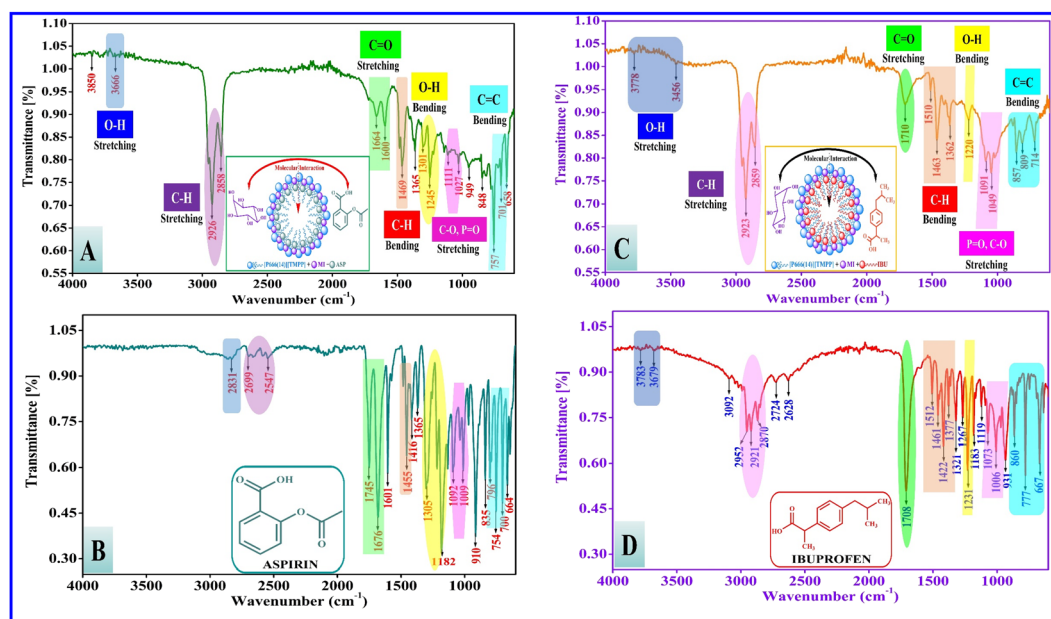


Fig. 6 FTIR spectra of [A] [P666(14)][TMPP] + MI + ASP, [B] ASP, [C] [P666(14)][TMPP] + MI + IBU, and [D] IBU.



which indicates a  $7\text{ cm}^{-1}$  shift in IR frequency. The  $[\text{C}=\text{C}]$  bending is observed at  $806\text{ cm}^{-1}$  and is shifted to  $857\text{ cm}^{-1}$ , which indicates a  $51\text{ cm}^{-1}$  shift in IR frequency. The  $[\text{C}-\text{H}]$  bending (disubstituted benzene) is observed at  $754\text{ cm}^{-1}$  and is shifted to  $809\text{ cm}^{-1}$ , which indicates a  $55\text{ cm}^{-1}$  shift in IR frequency.

Ultimately, PIL interaction with MI and ASP/IBU can break down and modify of the hydrogen bond structure. Numerous hydrogen bonds are produced in the ASP, and IBU has  $\text{OH}^-$  and  $-\text{COO}^-$  groups. The interaction between PIL and MI/IBU, shown the IR frequency are  $223\text{ cm}^{-1}$  and  $144\text{ cm}^{-1}$ . The  $\text{OH}^-$  and  $-\text{COO}^-$  polar groups of myo-inositol synchronize with hydrogen bonding when the ASP/IBU bind with phosphonium ions. These possible molecular interactions are shown in Scheme 2. The C–O stretching bands in the ASP exhibit two strong peaks at  $1745\text{ cm}^{-1}$  and  $1676\text{ cm}^{-1}$ , and they display two broad bands at  $1664\text{ cm}^{-1}$  and  $1600\text{ cm}^{-1}$  following irradiation. The C–O stretching bands in the case of IBU have bandwidth at  $1710\text{ cm}^{-1}$  following irradiation, but the first feature is a strong peak at  $1708\text{ cm}^{-1}$ . PIL radiation also results in significant changes in C–O vibrations, suggesting that radiation-induced distortion of the C–O-containing hydrogen bond networks occurred. These findings suggest that when the two samples were exposed to radiation, the hydrogen bond structure dissolved and reorganized. The fingerprint region underwent changes in the peak locations of many bands as well as a shift in the relative intensity. The  $1470\text{--}1469\text{ cm}^{-1}$  band experienced the relative intensity at the  $1455\text{--}1422\text{ cm}^{-1}$  band has risen. The C=C bending shown the IR frequency is  $835\text{ cm}^{-1}$  and  $860\text{ cm}^{-1}$  regions and is shifted to  $848\text{ cm}^{-1}$  and  $857\text{ cm}^{-1}$ , respectively.

## 4. Conclusions

The molecular interaction of a phosphonium-based ionic liquid (PIL) such as trihexyltetradecylphosphonium bis(2,4,4-trimethylpentyl)phosphinate ( $[\text{P666}(14)]\text{[THPP]}$ ) with myo-inositol (MI) and NSAIDs, *i.e.*, aspirin (ASP) and ibuprofen (IBU), was studied with the help of surface tension, conductivity, colorimetry, viscometry, dynamic light scattering (DLS) and FTIR techniques. The CMC value of PIL is decreased with an increasing the concentration of MI (mM), and its highest impact was at 2.0 mM of MI, and similar types of results were observed with the MI-ASP/IBU system. The conformational study of CMC dealt with conductometry, colorimetric and DLS methods. The spontaneity of the micellization and adsorption processes of different systems was due to changes in more negative  $\Delta G_m^\circ$  and  $\Delta G_{\text{ads}}^\circ$  values. Rheological parameters, such as relative, reduced and intrinsic viscosity, were revealed for the PIL with various concentrations of MI-ASP/IBU systems by viscometry. The PIL + MI + IBU system has a more viscous and elastic tendency, as shown by this rheological measure, which suggests the stability of the system. The FTIR data showed that the MI + IBU system has good agreement with PIL compared to MI + ASP. MI has been utilized as a co-solvent for the entire system that can help bind PIL and NSAIDs. In agreement with the FTIR and DLS results, it was shown that PIL with MI-ASP/

IBU causes compositional changes. Consequently, we may say that using an appropriate PIL will help have a positive impact on drug delivery and reduce the deficiencies of drugs. The current research will have effects on pharmaceutical sciences, molecular biology, and drug delivery.

## Author contributions

The manuscript was written through the contributions of all authors. All authors have approved the final version of the manuscript.

## Conflicts of interest

There are no conflicts to declare.

## Acknowledgements

The authors thank Dr Manmohan L. Satnami, School of Studies in Chemistry, Pt. Ravishankar Shukla University, Raipur (C.G.) for providing the experimental facilities to measure the aggregate size distribution obtained from DLS and Mr Dilip Kumar Chandra, Department of Biotechnology, National Institute of Technology (NIT), Raipur, Chhattisgarh India for providing the experimental facilities to measure the stretching frequency of the micellar complex from FTIR. The authors are grateful to the HOD, Department of Chemistry (MSS), MATS University Raipur, Chhattisgarh, India for providing laboratory facilities.

## References

- 1 A. Celebioglu and T. Uyar, Hydrocortisone/cyclodextrin complex electrospun nanofibers for a fast-dissolving oral drug delivery system, *RSC Med. Chem.*, 2020, **11**, 245–258.
- 2 A. Schittny, S. Philipp-Bauer, P. Detampel, J. Huwyler and M. Puchkov, Mechanistic insights into effect of surfactants on oral bioavailability of amorphous solid dispersions, *J. Controlled Release*, 2020, **320**, 214–225.
- 3 X. J. Cheng, J. X. Gu, Y. P. Pang, J. Liu, T. Xu, X. R. Li, Y. Z. Hua, K. A. Newell, X. F. Huang, Y. Yu and Y. Liu, Tacrine–hydrogen sulfide donor hybrid ameliorates cognitive impairment in the aluminum chloride mouse model of alzheimer's disease, *ACS Chem. Neurosci.*, 2019, **10**, 3500–3509.
- 4 S. Ahmadi, H. A. Dabbagh, P. Grieco and S. Balalaie, A cystine-based dual chemosensor for fluorescentcolorimetric detection of  $\text{CN}^-$  and fluorescent detection of  $\text{Fe}^{3+}$  in aqueous media: Synthesis, spectroscopic, and DFT studies, *Spectrochim. Acta, Part A*, 2020, **228**, 117696.
- 5 P. Sappidi, M. Maurya, K. E. O'Harra, J. E. Bara and C. H. Turner, Molecular simulations and experimental studies of the structural properties of imidazolium ionenes with butyl and decyl spacers solvated in 1-ethyl-3-methylimidazolium bistriflimide, *J. Ionic Liquids*, 2022, **2**, 100013.
- 6 B. K. Chennuri, V. Losetty, K. Sreenivasulu, R. L. Gardas and K. Sivakumar, Analysis of thermophysical properties of





- binary mixtures of N -phenyl ethanolammonium based protic ionic liquids with water and ethanol solvents, *J. Ionic Liquids*, 2022, **2**, 100015.
- 7 D. Ausín, J. J. Parajó, J. L. Trenzado, L. M. Varela, O. Cabeza and L. Segade, Influence of small quantities of water on the physical properties of alkylammonium nitrate ionic liquids, *Int. J. Mol. Sci.*, 2021, **22**, 7334.
  - 8 M. K. Banjare, K. Behera, M. L. Satnami, S. Pandey and K. K. Ghosh, Self-assembly of a short-chain ionic liquid within deep eutectic solvents, *RSC Adv.*, 2018, **8**, 7969.
  - 9 I. Rodríguez-Escontrela, I. Rodríguez-Palmeiro, O. Rodríguez, A. Arce and A. Soto, Phase behavior of the surfactant ionic liquid trihexyltetradecylphosphonium bis(2,4,4-trimethylpentyl)phosphinate with water and dodecane, *Colloids Surf., A*, 2015, **480**, 50–59.
  - 10 W. D. Amith, J. C. Araque and C. J. Margulis, Ether tails make a large difference for the structural dynamics of imidazolium-based ionic liquids, *J. Ionic Liquids*, 2022, **2**, 100012.
  - 11 R. Md Moshikur, Md. R. Chowdhury, M. Moniruzzaman and M. Goto, Biocompatible ionic liquids and their applications in pharmaceuticals, *Green Chem.*, 2020, 1–25.
  - 12 O. A. El Seoud, N. Keppeler, N. I. Malek and P. D. Galgano, Ionic liquid-based surfactants: recent advances in their syntheses, solution properties, and applications, *Polymers*, 2021, **13**, 1100.
  - 13 S. N. Pedro, C. S. R. Freire, A. J. D. Silvestre and M. G. Freire, Ionic liquids in drug delivery, *Encyclopedia*, 2021, **1**, 324–339.
  - 14 D. Kumar, M. U. D. Parray, F. A. Wani, N. Dohare, M. Ali, R. Patel and A. B. Khan, Deciphering the role of alkyl chain length on interaction analysis of antidepressant drug-cationic surfactants in imidazolium based ionic liquid, *J. Iran. Chem. Soc.*, 2022, **19**, 2449–2457.
  - 15 M. K. Banjare, K. Behera, M. L. Satnami, S. Pandey and K. K. Ghosh, Supra-molecular inclusion complexation of ionic liquid 1-butyl-3-methylimidazolium octylsulphate with  $\alpha$ - and  $\beta$ -cyclodextrins, *Chem. Phys. Lett.*, 2017, 1–25.
  - 16 W. Zhuang, C. Zhao, Y. Pan and Q. Li, Self-assembly of an imidazolium surfactant in aprotic ionic liquids 2. more than solvents, *Soft Matter*, 2021, **17**, 3494–3502.
  - 17 R. L. Pérez, C. E. Ayala, M. M. Opiri, A. Ezzir, G. Li and I. M. Warner, Recycling thermoset epoxy resin using alkyl-methyl-imidazolium ionic liquids as green solvents, *ACS Appl. Polym. Mater.*, 2021, **3**, 5588–5595.
  - 18 M. S. Lone, S. Afzal, O. A. Chat, V. K. Aswal and A. A. Dar, Temperature- and composition-induced multiarchitectural transitions in the catanionic system of a conventional surfactant and a surface-active ionic liquid, *ACS Omega*, 2021, **6**, 11974–11987.
  - 19 M. Lee, S. L. Perry and R. C. Hayward, Complex coacervation of polymerized ionic liquids in non-aqueous solvents, *ACS Polym. Au*, 2021, **1**, 100–106.
  - 20 M. Koundal, A. K. Singh and C. Sharma, Analysis on the effect of imidazolium ionic liquid as a modulator of corrosion inhibition of anionic surfactant sodium dodecyl sulfate (SDS) on mild steel in sodium chloride solution, *J. Mol. Liq.*, 2022, **350**, 118561.
  - 21 L. K. S. Tanwar, S. Sharma and K. K. Ghosh, Interaction of an imidazolium based ionic liquid with antidepressant drugs: a physicochemical analysis, *Colloids Surf., A*, 2022, **636**, 128159.
  - 22 S. Chatree, N. Thongmaen, K. Tantivejkul, C. Sitticharoon and I. Vucenik, Role of inositols and inositol phosphates in energy metabolism, *Molecules*, 2020, **25**, 5079.
  - 23 S. Mukherjee, J. Haubner and A. Chakraborty, Targeting the inositol pyrophosphate biosynthetic enzymes in metabolic diseases, *Molecules*, 2020, **25**, 1403.
  - 24 J. S. Ramos-Figueroa, H. B. Aamudalapalli, R. C. Jagdhane, J. Smith and D. R. J. Palmer, Preparation and application of <sup>13</sup>C-labeled myo-inositol to identify new catabolic products in inositol metabolism in lactobacillus casei, *Biochemistry*, 2020, **59**, 2974–2985.
  - 25 X. Su, W. Dohle, S. J. Mills, J. M. Watt, A. M. Rossi, C. W. Taylor and B. V. L. Potter, Inositol adenophostin: convergent synthesis of a potent agonist of d-myo-inositol 1,4,5-trisphosphate receptors, *ACS Omega*, 2020, **5**, 28793–28811.
  - 26 S. J. Mills, A. M. Rossi, V. Konieczny, D. Bakowski, C. W. Taylor and B. V. L. Potter, d-chiro-Inositol ribophostin: a highly potent agonist of d-myo-inositol 1,4,5-trisphosphate receptors: synthesis and biological activities, *J. Med. Chem.*, 2020, **63**, 3238–3251.
  - 27 X. Li, C. Gu, S. Hostachy, S. Sahu, C. Wittwer, H. J. Jessen, D. Fiedler, H. Wang and S. B. Shears, Control of XPR1-dependent cellular phosphate efflux by insp(8) is an exemplar for functionally-exclusive inositol pyrophosphate signaling, *Proc. Natl. Acad. Sci. U. S. A.*, 2020, **117**, 3568–3574.
  - 28 A. S. Laganà, V. Unfer, S. Garzon and M. Bizzarri, Role of inositol to improve surfactant functions and reduce IL-6 levels: a potential adjuvant strategy for sars-cov-2 pneumonia?, *Med. Hypotheses*, 2020, **144**, 110262.
  - 29 C. Fan, W. Liang, M. Wei, X. Gou, S. Han and J. Bai, Effects of d-chiro-inositol on glucose metabolism in db/db mice and the associated underlying mechanisms, *Front. Pharm.*, 2020, **11**, 354.
  - 30 G. Formoso, M. P. A. Baldassarre, F. Ginestra, M. A. Carlucci, I. Bucci and A. Consoli, Inositol and antioxidant supplementation: safety and efficacy in pregnancy, *Diabetes/Metab. Res. Rev.*, 2019, **35**, e3154.
  - 31 Z. Song, Q. Yu, M. Cai, G. Huang, M. Yao, D. Li, Y. Liang, M. Fan and F. Zhou, Green ionic liquid lubricants prepared from anti-inflammatory drug, *Tribol. Lett.*, 2015, **60**, 1–11.
  - 32 Y. Wang, Q. Yu and M. Cai, Ibuprofen-based ionic liquids as additives for enhancing the lubricity and antiwear of water-ethylene glycol liquid, *Tribol. Lett.*, 2017, **65**, 55.
  - 33 H. Wu, Z. Deng, B. Zhou, M. Qi, M. Hong and G. Ren, Improved transdermal permeability of ibuprofen by ionic liquid technology: Correlation between counterion structure and the physicochemical and biological properties, *J. Mol. Liq.*, 2019, **283**, 399–409.



